

Numerical Methods for Determination of Rayleigh-Taylor Mixing

E. George*, J. Glimm*, J. Grove†, X.-L. Li*,
A. Marchese*, D. Sharp†, and Z.-L. Xu*

* *Department of Applied Mathematics and Statistics, SUNY at Stony Brook,
Stony Brook, NY 11794-3600*

† *Los Alamos National Laboratory
Los Alamos, NM 87545*

Abstract

We present a Rayleigh-Taylor mixing rate simulation with an acceleration rate falling within the range of experiments. The simulation uses front tracking to prevent interfacial mass diffusion. We present evidence to support the assertion that the lower acceleration rate found in untracked simulations is caused, at least to a large extent, by a reduced buoyancy acceleration due to numerical interfacial mass diffusion. Quantitative evidence includes results from a time dependent Atwood number analysis of the untracked simulation, which yields a renormalized mixing rate coefficient for the untracked simulation in agreement with experiment.

Since Read and Youngs [5, 6] published the first experimental study of Rayleigh-Taylor instability with a randomly perturbed fluid interface, attention has been drawn to the non-dimensional acceleration rate of the bubble envelope.

$$h(t) = \alpha A g t^2, \tag{1}$$

where h is the height of the bubble envelope, A is the Atwood number, g is the gravity and t is time. Read and Youngs show that the acceleration rate α is almost a constant, with $\alpha \sim 0.063 - 0.077$ in 3-D experiments. The experiments have been repeated by various authors with different apparatus, and similar values of α have been obtained; we mention the experiments of Dimonte and Schneider [1, 2, 3], giving $\alpha = 0.05 \pm 0.01$.

Most researchers report a time dependent, decreasing value for α , ranging from 0.015 to 0.03 from numerical simulations. These simulations are from computational codes using numerical schemes with interfacial mass diffusion. We have compared numerical simulations using a high resolution front tracking code *FronTier* with zero interfacial mass diffusion to our own simulations using an untracked TVD-level set code with interfacial mass diffusion similar to the others. We also introduce an analytic study of the effects of mass diffusion on buoyancy reduction and we predict the numerically observed reduction

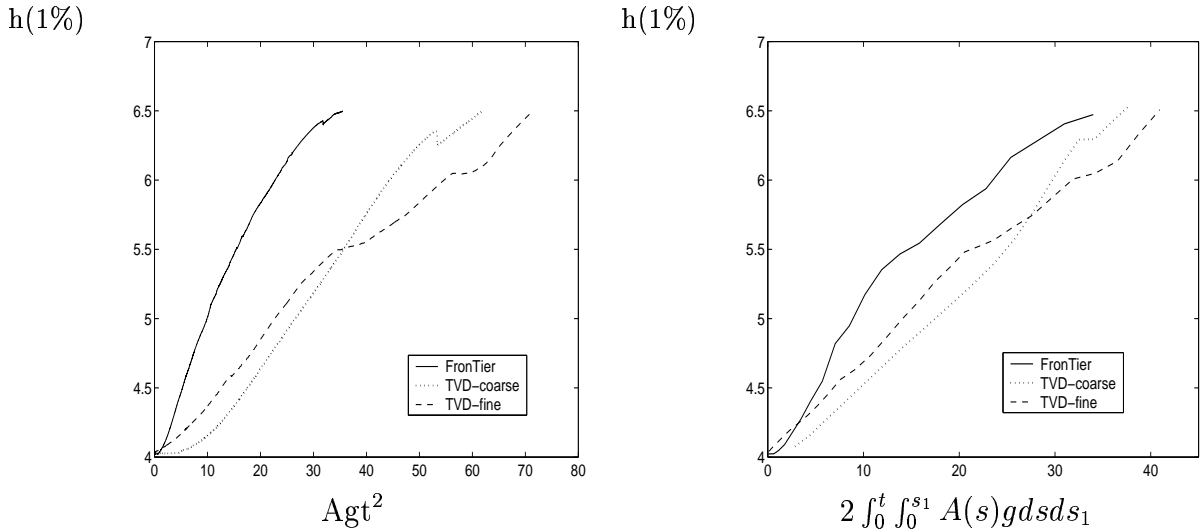


Figure 1: Mixing growth comparison of a *FronTier* (nondiffusive) with a TVD (diffusive) simulation. For the TVD simulation, two grid levels are shown, the coarser being $64^2 \times 128$. In all cases, h is the height of the 1% volume fraction contour, and the initial mean height of the interface is 4. Left: h vs. $A(t=0)gt^2$ for *FronTier* and TVD. Right: h vs. $2 \int_0^t \int_0^{s_1} A(s)g ds ds_1$ for *FronTier* and TVD. The solid line represents the *FronTier* simulation, the dashed line is the finer grid TVD simulation and the dotted line is the coarser grid TVD simulation.

in α for untracked simulations. Our main result is that all values of α (theory, experiment, simulation) are consistent if the diffusive calculation of α is renormalized to account for mass diffusion.

An earlier comparison shows that *FronTier* simulations produce values for α close to agreement with experiment while untracked TVD simulations produce low values for α [4]. These comparisons were limited in the simulation time and in the penetration depth of mixing achieved. Here we extend the comparison to a later time, comparable to most other simulations.

The $t = 0$ interface is constructed out of Fourier modes with random amplitudes and frequencies in the range of 8 – 16 modes per computational domain width. See [4] for further information concerning these simulations. The $2 \times 2 \times 8$ computational domain used here allows computationally efficient late time, deep penetration simulations. Within this computational aspect ratio, the Fourier mode numbers represent a balance between the conflicting requirements of spatial resolution, favoring low numbers of modes, and late time statistical validity, favoring large numbers of modes. The simulations used a

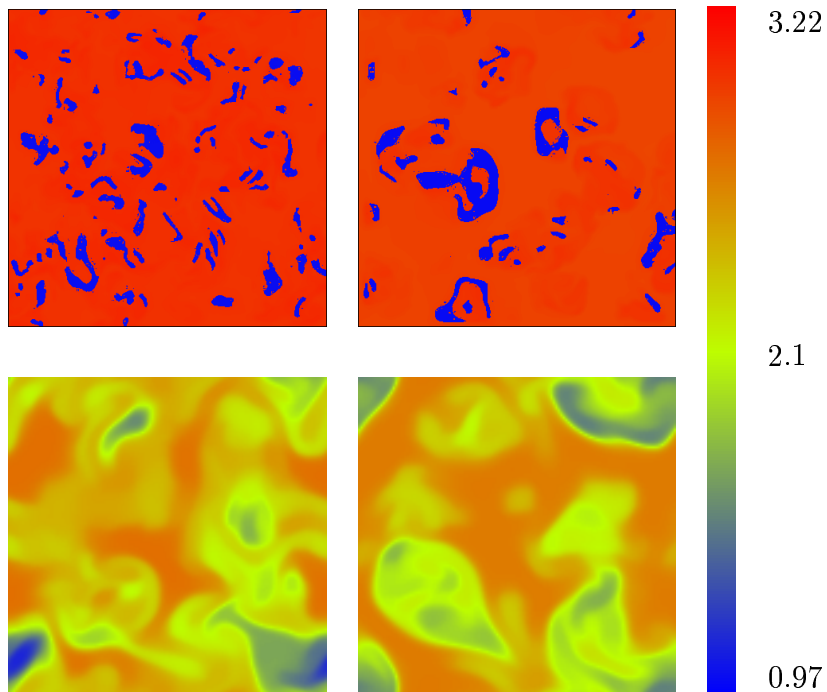


Figure 2: Cross sectional plots showing density on a common rainbow color scale. The light fluid is blue and the heavy fluid is red. The ratio of extreme density values is 3.3:1. The right frames show a higher slice in the z direction. Top: *FronTier*, bottom: TVD. The simulations are shown at comparable penetration distances, but at different times ($Agt^2 = 23$ for *FronTier*, $Agt^2 = 66$ for TVD).

$128^2 \times 512$ grid. Our simulations, thus balanced, have about $12^2 = 144$ initial bubbles and a grid resolution of about ten cells in each dimension per initial bubble.

A comparison of the mixing rates for the two simulations is shown in Fig. 1 (left), plotting bubble height h vs. Agt^2 . *FronTier* has a distinctly higher growth rate than does the interface mass diffusive TVD simulation. The value of $h(t)$ is the difference between the $t = 0$ bubble height and the time t bubble height. The latter quantity is defined in terms of a 1% volume fraction, i.e., the greatest height at which the fluid is 99% heavy and 1% light according to the front tracking front or the TVD level set. This definition is somewhat unstable statistically, and a few spurious oscillations associated with the definition were removed in the plots of Fig. 1.

Mass diffusion is a common feature of most untracked simulation codes. Due to the interpolation constraint, numerical schemes (finite difference, finite volume) can have only first order accuracy in their spatial derivatives near a discontinuity. For a contact discon-

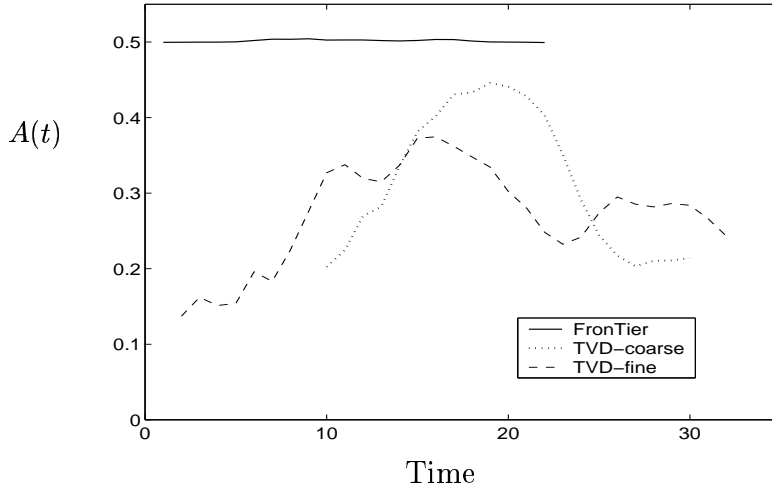


Figure 3: Time dependent A (Atwood number) for fine grid *FronTier*, fine grid TVD, and coarse grid ($64^2 \times 128$) TVD. At time $t = 0$, all three simulations have $A(t = 0) = 0.5$. This plot displays the reduced buoyancy of the diffusive TVD simulations as a function of time.

tinuity, the corresponding characteristic is linear for the wave equation of the Riemann invariant

$$\frac{\partial w}{\partial t} + u \frac{\partial w}{\partial x} = 0, \quad \text{where} \quad w = \rho - \frac{P}{c^2}, \quad (2)$$

and so the truncation error will spread to the interior region. A first order scheme is more diffusive if the time step Δt is much below the limit set by the CFL condition. Therefore the untracked simulation is particularly diffusive across the contact surface when the fluid is almost incompressible, because in such case, the Δt is dominated by the characteristic speed $|u \pm c|$ which is much larger than that of $|u|$.

In order to understand the difference between the two simulations, we compare the cross sectional density plots in a series of horizontal slices from the bubble (upper) portion of the mixing region. Fig. 2 shows the cross sectional density plots in these simulations. Observe that there is a substantial smearing-out of the density across the boundary between the two fluids in the untracked TVD simulation, while the *FronTier* simulation maintains a sharp boundary with a discontinuous density profile throughout the simulation. As a further difference, we note the fine scale structure size in the *FronTier* simulation in comparison to the TVD simulation.

We compute an effective Atwood number $A(t)$ as a function of time for the TVD simulations. This is determined from the highest and lowest densities in a horizontal slice, with the resulting time and space dependent Atwood number averaged over heights

| Method | α | Reference |
|---------------------------------------------|------------|--------------------------------|
| Experiment | 0.05-0.077 | [5, 6, 1, 2, 3] |
| <i>FronTier</i> simulation (unrenormalized) | 0.07 | This paper (Fig. 1, left); [4] |
| <i>FronTier</i> simulation (renormalized) | 0.07 | This paper (Fig. 1, right) |
| TVD simulation (unrenormalized) | 0.035 | This paper (Fig. 1, left) |
| TVD simulation (renormalized) | 0.06 | This paper (Fig. 1, right) |

Table 1: Values of α determined from experiment, theory, and simulation. All values are consistent except the unrenormalized TVD value (with α determined from a time independent $t = 0$ Atwood number).

in the upper third of the mixing zone at a fixed time to get an Atwood number dependent on time alone. In Fig. 3, we plot $A(t)$ vs. t for three simulations (fine and coarse grid TVD and fine grid *FronTier*). The time dependence of $A(t)$ in the *FronTier* simulation is caused purely by (small) compressibility effects. For the mass diffusive TVD simulation, the initial density contrast, $A(t = 0) = 0.5$, is almost completely washed out; the earliest time displayed shows $A(t = 2) \approx 0.15$. As new pure (heavy and light) fluid is injected into the mixing region, the effective Atwood number increases, but it is still reduced to about $A \approx 0.3$ on a time averaged basis, or nearly a 50% reduction relative to its initial value.

To compensate for the time dependent Atwood number $A(t)$, we define an effective alpha, $\alpha_{\text{eff}} \approx h/2 \int \int A(s) g ds dt$ (see Fig. 1, right). Specifically, α or α_{eff} is defined here as the slope of the straight line joining the beginning and end of the $h(t)$ curve in Fig. 1. This definition, although somewhat arbitrary, is conventional, and thus allows comparison to the results of others. We observe an improved comparison between *FronTier* and TVD and between TVD and experiment. Note that α_{eff} lies within the range of experimental values; see Table 1. On this basis, we can state that the diffusive buoyancy renormalization of α is capable of resolving existing discrepancies among simulations, between diffusive simulations and nondiffusive experiments, and with theory.

The reduced mixing rate due to unphysical numerical diffusion can be understood from Fig. 4. The left frame represents an immiscible bubble of radius r . The central and the right frame assume that this bubble is smeared out numerically to a radius R while the total mass inside the sphere of radius R is conserved. The buoyancy forces

$$f_1 = f_2 = \frac{4\pi r^3}{3}(\rho_H - \rho_L)g \quad (3)$$

for the bubbles in frames (a) and (c) are the same. However, due to the difference between the mass in the nondiffused bubble (a) and the diffused bubble (c), the two acceleration

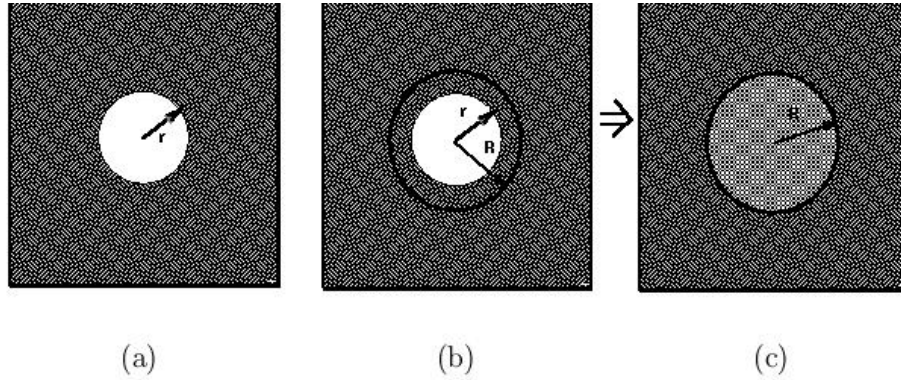


Figure 4: Left: Unmixed bubble of light fluid. Center: Unmixed bubble and heavy fluid mass which will be mixed with it. Right: Mixed bubble.

rates

$$a_1 = \frac{\rho_H - \rho_L}{\rho_L} g > a_2 = \frac{\rho_H - \rho_L}{\rho_L + \left(\frac{R^3}{r^3} - 1\right) \rho_H} g \quad (4)$$

are different. As a result of the mass diffusion, the buoyancy force is distributed to a larger amount of mass, thus reducing the acceleration of the bubble.

References

- [1] G. Dimonte. *Phys. Plasmas*, 6(5):2009–2015, 1999.
- [2] G. Dimonte and M. Schneider. *Phys. Rev. E*, 54:3740–3743, 1996.
- [3] G. Dimonte and M. Schneider. *Phys. Fluids*, 12:304–321, 2000.
- [4] J. Glimm, J. W. Grove, X. L. Li, W. Oh, and D. H. Sharp. *J. Comp. Phys.*, 169:652–677, 2001.
- [5] K. I. Read. *Physica D*, 12:45–58, 1984.
- [6] D. L. Youngs. *Physica D*, 12:32–44, 1984.